Macromolecular Rapid Communications
www.mrc-journal.de

Reconfigurable Polymer Shells on Shape-Anisotropic Gold Nanoparticle Cores

*Juyeong Kim, Xiaohui Song, Ahyoung Kim, Binbin Luo, John W. Smith, Zihao Ou, Zixuan Wu, and Qian Chen**

Reconfigurable hybrid nanoparticles made by decorating flexible polymer shells on rigid inorganic nanoparticle cores can provide a unique means to build stimuli-responsive functional materials. The polymer shell reconfiguration has been expected to depend on the local core shape details, but limited systematic investigations have been undertaken. Here, two literature methods are adapted to coat either thiol-terminated polystyrene (PS) or polystyrene-poly(acrylic acid) (PS-*b*-PAA) shells onto a series of anisotropic gold nanoparticles of shapes not studied previously, including octahedron, concave cube, and bipyramid. These core shapes are complex, rendering shell contours with nanoscale details (e.g., local surface curvature, shell thickness) that are imaged and analyzed quantitatively using the authors' customized analysis codes. It is found that the hybrid nanoparticles based on the chosen core shapes, when coated with the above two polymer shells, exhibit distinct shell segregations upon a variation in solvent polarity or temperature. It is demonstrated for the PS-*b*-PAA-coated hybrid nanoparticles, the shell segregation is maintained even after a further decoration of the shell periphery with gold seeds; these seeds can potentially facilitate subsequent deposition of other nanostructures to enrich structural and functional diversity. These synthesis, imaging, and analysis methods for the hybrid nanoparticles of anisotropically shaped cores can potentially aid in their predictive design for materials reconfigurable from the bottom up.

1. Introduction

Hybrid nanomaterials incorporating inorganic metal nanoparticle cores and organic polymer shells have shown intriguing coupled properties[1–4] as well as applications in diagnosis,[5] drug delivery,[6,7] catalysis,[8] and self-assembly.[9–11] Additionally, polymer shells have conformational flexibility and exhibit shape reconfiguration upon external stimuli, not accessible to rigid metal nanoparticle cores alone.[12–14] The reconfiguration modulates nanoparticle surface, leading to dynamic control over nanoparticle interactions,[15–17] assembly,[18,19] and phase transitions[20–22] of nanocomposites with desired properties. For example, the polystyrene (PS) shell on PS-coated gold nanospheres was shown to shift its spatial distribution into a "Janus-like" geometry upon a solvent polarity change.[13] Such polymer shell shape shifting can serve as a bottom-up surface patterning method at the single nanoparticle level, to allow nanoscale lithography[23] and directed nanoparticle self-assembly[24,25] for developing functional nanomaterials.

In these systems, the shape of metal nanoparticle core determines the local surface curvature of the surface[26] that polymer shell dwells upon, which renders a spatially uneven polymer packing density[27,28] and interpolymer interactions.[29] Earlier work on PS-coated gold nanoparticles show that the gold nanocubes and spheres have distinct PS shell shapes upon reconfiguration.[13,14] Work on block copolymer, polystyrene-poly(acrylic acid) (PS-*b*-PAA)-coated gold nanorods show that the polymer shell segregates towards the rod center upon heating.[30] However, the dependence of polymer shell reconfiguration on the shape of the cores has not been systematically investigated due to the limited core shapes studied and the lack of quantitative characterization of the shape details of both the core and the polymer shell.[13,14]

Here we use shape-anisotropic gold polyhedra as the model metal nanoparticle core, and adapt for the core particles the methods of coating thiolated PS or PS-*b*-PAA demonstrated earlier for other shapes. Specifically, we use gold core nanoparticles grown from a universal seeded growth,[31] in which anisotropic shapes with readily tunable sizes and

Dr. J. Kim, Dr. X. Song, A. Kim, B. Luo, J. W. Smith, Z. Ou, Z. Wu, Prof. Q. Chen
Department of Materials Science and Engineering
University of Illinois at Urbana-Champaign
Urbana, IL 61801, USA
E-mail: qchen20@illinois.edu
Dr. J. Kim, Dr. X. Song, Prof. Q. Chen
Frederick Seitz Materials Research Laboratory
University of Illinois at Urbana-Champaign
Urbana, IL 61801, USA
Prof. Q. Chen
Department of Chemistry
University of Illinois at Urbana-Champaign
Urbana, IL 61801, USA
Prof. Q. Chen
Beckman Institute for Advanced Science and Technology
University of Illinois at Urbana-Champaign
Urbana, IL 61801, USA
The ORCID identification number(s) for the author(s) of this article can be found under https://doi.org/10.1002/marc.201800101.

DOI: 10.1002/marc.201800101

great monodispersity can be obtained from the same seed source for systematic study. The core shapes we choose are as follows. Cubes are used as a comparison with previous work on PS-coated cubes,[14] which were synthesized using a different method with ligands different from ours (hexadecylpyridinium chloride monohydrate (CPC) in our work and hexadecyltrimethylammonium bromide (CTAB) in previous work[14]). In addition, nonstudied shapes such as octahedra, concave cubes, and bipyramids are also studied by us as core particles, which cover a wide range of local surface curvature values, from convex, flat to concave. We examine and quantify the shell reconfiguration behaviors on these various core shapes under different stimuli. For different core shapes, the polymer patterns after segregation are different. Interestingly, we find a consistent trend that the PS shells on gold nanoparticles tend to segregate towards the high surface curvature sites of the core particle with different core shapes upon addition of more polar solvents, while the PS-*b*-PAA shells segregate to low surface curvature sites of the core particles upon heating. In other words, these two types of polymer coating generate complimentary segregated patterns on core particle surface. In addition, to potentially enrich the functionality of the hybrid nanoparticles, we integrate and validate a gold seeding method to PS-*b*-PAA-coated particles, and find that the gold seeded particles still maintain the predicted shell reconfiguration. This opens doors for further use of the gold seeds as active sites for further growth of gold nanowires,[32] nanoplates,[33] and nanorods[34] for incorporation of more functions, in our reconfigurable building blocks. We establish an imaging and analysis platform to map the local curvatures of the nanoparticle core and polymer shell, the local thickness of the polymer shell at nanometer resolution, to quantify the shape shifting of polymer shell, which can generalize to other nanoparticle–polymer hybrid systems.

2. Results and Discussion

2.1. Shape-Dependent Reconfiguration of PS-Shelled Octahedral and Cube Nanoparticles

Here we use two types of anisotropic gold nanoparticles as the core, octahedra (49.5 ± 1.7 nm) and cubes (60.3 ± 2.0 nm), prepared in high monodispersity following the universal seeded-growth method[31] (Figure S1, Supporting Information). These two shapes belong to the same symmetry class as dual polyhedra but with distinct faceting details.[35] The gold octahedron is composed of eight {111} facets, while the gold cube consists of six {100} facets, both with round vertices from synthesis (**Figure 1**). We first adapted the thiolated PS coating methods to these gold nanoparticles[13,14] with modification, where higher concentrated nanoparticle solution was used to increase the yield. The PS-coated nanoparticles were then imaged under an optimized TEM condition at 100 kV. The polymer shell is clearly seen as a light shadow enveloping gold nanoparticle core of darker contrast (Figure 1c–e), in the absence of staining agents which avoids complications. The PS shell stays stable under TEM accelerating voltages of 100 and 200 kV, but becomes dilated at an accelerating voltage of 300 kV due to high-voltage electron beam (Figure S2, Supporting Information).

In the initial nonpolar solvent of tetrahydrofuran, the polymer coating on the gold cores is uniform. As shown in Figure 1d, the PS-coated octahedral nanoparticles have one {111} facet sitting on the TEM grid, with their shapes matched with a hexagon projected from a 3D octahedron (the red hexagon in Figure 1a). Based on various projected 2D views of these octahedral nanoparticles (Figure 1d, Figure S3, Supporting Information), we conclude that they are uniformly coated with PS. This observation is consistent with previous work on spherical and cube cores,[13,14] in which tetrahydrofuran is seen as a "good solvent" for PS; solvent–polymer attraction is stronger than polymer–polymer attraction,[36] so that PS molecules stay extended and homogeneous on octahedral particle surface. We observe the same uniform PS coating for the cube hybrid nanoparticles with a shell thickness of ≈10 nm, consistent with previous reports despite the different cube synthesis used (Figure 1l).

PS shell reconfiguration is induced by dispersing these hybrid nanoparticles in polar solvent (e.g., a mixture of dimethylformamide and water, 1 vol% of water) following a literature method,[14] and was quantified based on local surface curvature and local shell thickness. Upon this solvent change, we observe that the uniformly distributed PS shell undergoes a segregation process into surface pinned domains on the octahedral nanoparticles, similar to earlier work on cube cores[14] (Figure 1d,e). This surface segregation is associated with an ensemble change in the UV–Vis spectra of the gold nanoparticle solution. As shown in Figure 1b, gold octahedral cores experience a slight red shift (10 nm) in the absorption peak after PS shell formation and then after segregation (5 nm), indicating a decent yield in these postsynthesis modification steps. Due to the complexity of the 3D octahedral shape, we quantified the extent of shell reconfiguration by outlining the contours of the imaged PS shells and the gold cores as shown in Figure 1d,e. The contour colors are coded based on calculated local curvature (the inverse of the radius of the best-fitted circle).[37] The singled-out polymer shell region is color-coded by the local thickness (Figure 1f,g), defined at each point as the diameter of the largest circle that can contain a shell point and remain within the bounds of the shell. Before segregation, the PS shells have very similar local surface curvature distribution to that of the gold octahedral core (Figure 1h,i). The local thickness peaked at 10 nm, with an extended tail into 13 nm (Figure 1j), consistent with the projected 2D shape of the polymer shell that we contoured. After immersed in polar solvents, the local surface curvature distribution of the PS shell shifts to higher values (Figure 1i), as the PS shells segregate at six vertices of the octahedron into six regions. The local surface curvature distribution expands to a broad range of positive and negative values, demonstrating quantitatively the patchy nature of the segregated regions—spatially connected continuously via concave and convex regions. The local thickness profile, on the other hand, has a wider distribution after segregation, with a slight shift of the major peak to a thickness of 7 nm and a new peak at about 1 nm (Figure 1j). The existence of the new peak validates the existence of extended regions covered with very few PS

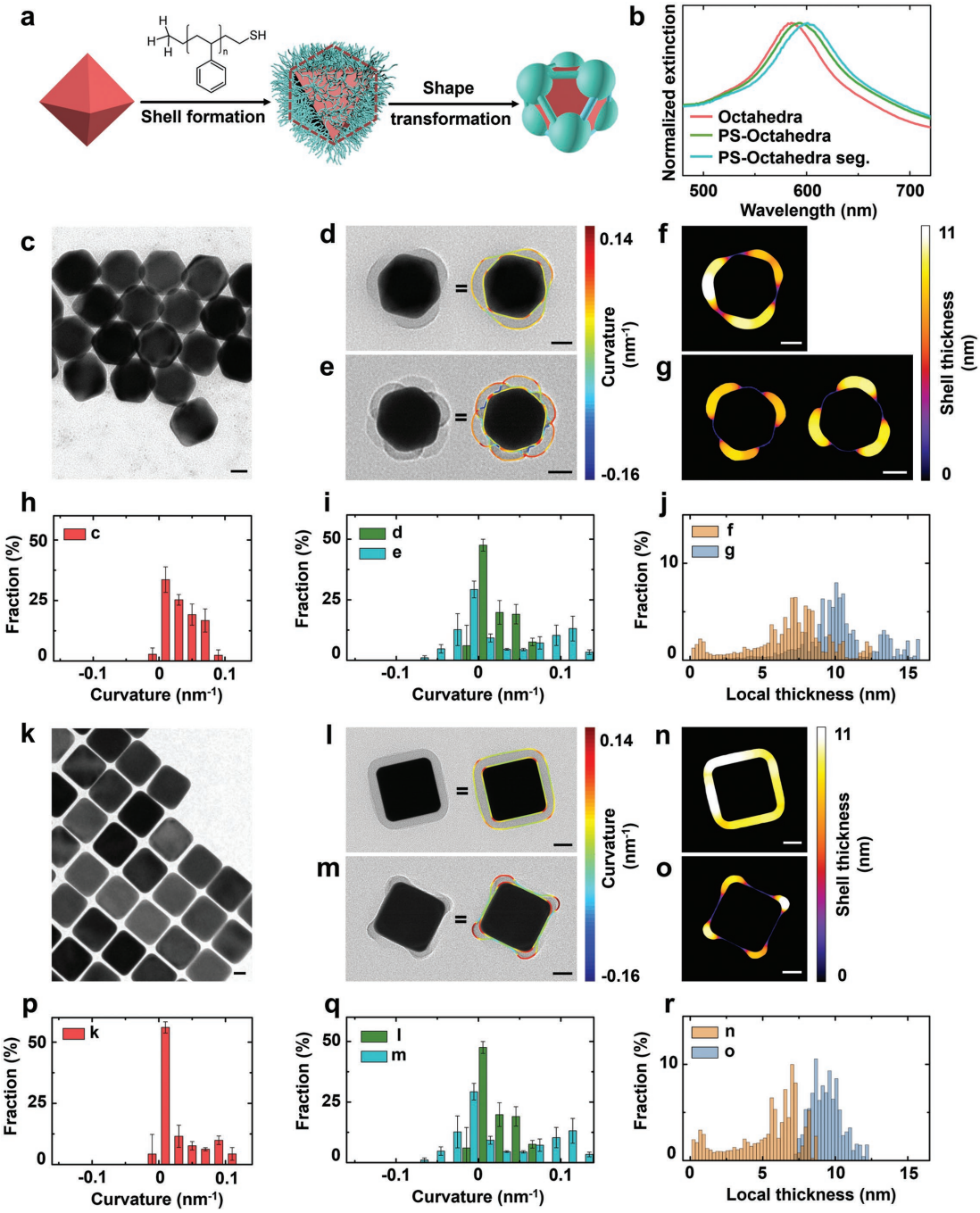

Figure 1. PS shell decoration and reconfiguration on gold polyhedral nanoparticles. a) Schematic of the coating and triggering of segregation of PS polymer shells onto gold octahedral nanoparticles as an example. The PS polymers are colored as emerald, and the representative segregation patterns (simplified) after shell segregation are shown at the corners of the octahedron. The dotted line in the middle scheme indicates the 2D projected outline of the octahedron. b) UV–Vis spectra of gold octahedra solution before the PS shell formation (red), right after the PS shell formation (olive), and after PS shell segregation (cyan). TEM images of c) as-synthesized gold octahedral nanoparticles, d) PS-coated ones, and e) PS-coated ones after shell segregation. d,e) are overlaid with surface contours color coded according to local surface curvature values. The singled-out PS shell region on octahedral core colored-coded according to the local thickness values f) before and g) after polymer shell segregation. The local surface curvature distributions of h) as-synthesized octahedra nanoparticles, i, olive) PS shells before and i, cyan) after segregation. j) The local thickness of PS shells before (blue) and after (orange) segregation. For each local surface curvature graph, we did the full contouring of both the gold core and polymer shell of about eight particles imaged at the same orientation (so that we can accumulate the measurements), which show a high consistency in the overlaid graphs in Figure S4 (Supporting Information). TEM images of k) as-synthesized gold cube nanoparticles, l) PS-coated ones and m) PS-coated ones after shell segregation. l,m) are overlaid with surface contours color coded according to local surface curvature values. The singled-out PS shell region on cube core colored-coded according to the local thickness values n) before and o) after polymer shell segregation. The local surface curvature distributions of p) as-synthesized gold cube nanoparticles, q, olive) PS shells before and q, cyan) after segregation. r) The local thickness of PS shells before (blue) and after (orange) segregation. Scale bars: 20 nm.

molecules, again consistent with the patchy, segregated nature of the PS regions.

The hybrid PS-coated cube nanoparticles undergo a similar PS shell segregation to the edges and vertices which have high local surface curvature, while less amount of the PS shell remains on flat {100} facets (Figure 1k–m), consistent with previous work[14] despite different cube synthesis. Compared with octahedral nanoparticles, the local surface curvature distribution of the segregated PS shells on cubes show more populated negative curvature values, i.e., more concave regions (Figure 1p,q). This difference might be attributed to the exact shape of the vertices (dihedral angle = 109.47°, four faces met at each vertex for octahedra, and dihedral angle = 90°, three faces met at each vertex for cubes), or due to the difference in the packing density of polymers on different facets. The local thickness distribution similarly shows that the peak at the small value is of a higher portion than that for the octahedral particles (Figure 1n,o,r).

It is clear that two differently shaped cores give rise to different, quantifiable segregation patterns with distinct nanoscale morphology details. Note that since polymer segregation is a thermodynamic-driven process from a competition between surface energy and stretching energy of polymers,[13,36] we expect that the core nanoparticle shape can potentially lead to predictable control of the segregation pattern, which can be of crucial importance to control the internanoparticle interactions. In particular, the segregated polymer regions can serve as attractive patches, with their size and shape determine the "valency" of particles, namely the allowed geometric arrangements for particles to connect and assemble. The segregation at the particle corners carries unique potential to direct assembly into nonclosely packed, hierarchical nanocomposite materials.[12,38]

2.2. Quantifying Polymer Shell Shapes (Local Surface Curvature and Thickness) on Anisotropic Nanoparticles

For the hybrid nanoparticles, polymer shell shape is the key parameter bridging particle core shape, segregation condition, and potential use as patchy particles for building into higher-order structures. For example, previous experimental and theoretical work have shown that spherical particles with attractive patches have distinct interparticle interactions and final assembled structures as the size, shape, number and spatial arrangements of the patches vary.[12,38] In addition, making shell shapes quantifiable can also facilitate fundamental understanding of how polymer shells adopt different shapes on curved core surfaces for predictive engineering.

To achieve the shell shape quantification, we adopted the surface contour analysis used by us on gold triangular prisms[37] and gold rod etching,[39] but modified extensively to optimize for polymer shell contouring and to elucidate the local shell thickness profile which is relevant in the context of polymer coating. Below we detail the work flow (**Figure 2**). All the TEM images are processed automatically using functions in an open-source software package ImageJ with minor manual adjustment. Gold nanoparticle cores have high contrast under TEM due to large atomic number, while polymer shells have low TEM contrast. One of the important modifications in our contour finding is to recognize the contours of both components by applying different image processing conditions for each component. Take the relatively simple cube hybrid nanoparticles as an example (Figure 2a,b). A low threshold value on gray scale produces a binary (black and white) image to capture the gold core shape (binary condition 1 in Figure 2b). Next by increasing the threshold, the lower-contrast polymer shell was recognized in the other binary image (binary condition 2 in Figure 2b). Depending on the edge roughness of the black shape in the binary image, a "median filter" with a few pixels' size or a removing outlier tool was applied to make the contour line smooth for computing the local curvature values. Furthermore, we applied the "find edges" function in ImageJ to the binary images to identify the contour lines and extract the coordinates of points comprising the lines. The line coordinates were imported into our customized MATLAB codes to compute local curvature values. In the code, two independent variables were manipulated to control the number of neighboring points used for smoothing the contour and for calculating the locally best-fitted circles. Lastly, the identification of both the gold core and the polymer shell contours enables us to single out and analyze the shell regions and to quantify the local shell thickness distribution of the segregated shell regions using a built-in function in ImageJ, which spatially varies and describes the shape of the patch.

The contour-finding becomes complicated for the octahedron hybrid nanoparticles after polymer segregation, where the segregated regions at different heights do not overlap. In comparison, cubes are a simpler case as their facets either sit flat or perpendicular to the TEM grid, so that the segregated polymer patches of the bottom cube facet overlay perfectly with those on the top. As shown in Figure 2c,d, the six patches after shell segregation have three on one plane and the other three on the other, yet all project individually onto the 2D TEM image. A plain analysis of the 2D image can result in incorrect assignment of the patch boundaries. Instead, based on the 3D geometry of the octahedron, we distinguish the polymer shells on different planes by their gray values. As shown in the gray value distribution (Figure 2e), one set of three segregated shell regions in the triangular configuration has higher contrast than the rest set of three, which are identified automatically as on the same plane (Figure 2d). This arrangement is consistent with the vertices of the octahedron (three on top and the other three at the bottom, positioned not in registry). Three polymeric patches on one plane are first eliminated to obtain the clear boundary of the other three, to reveal the shape, the local curvature distribution as well as the local thickness of each projected patch.

2.3. Reconfigurable PS-*b*-PAA Shells on Anisotropically Shaped Gold Nanoparticles

Besides using the thiolated PS as the polymer shell for shape-anisotropic gold cores, we adopted the shelling of amphiphilic block copolymers, PS-*b*-PAA, to core shapes not explored

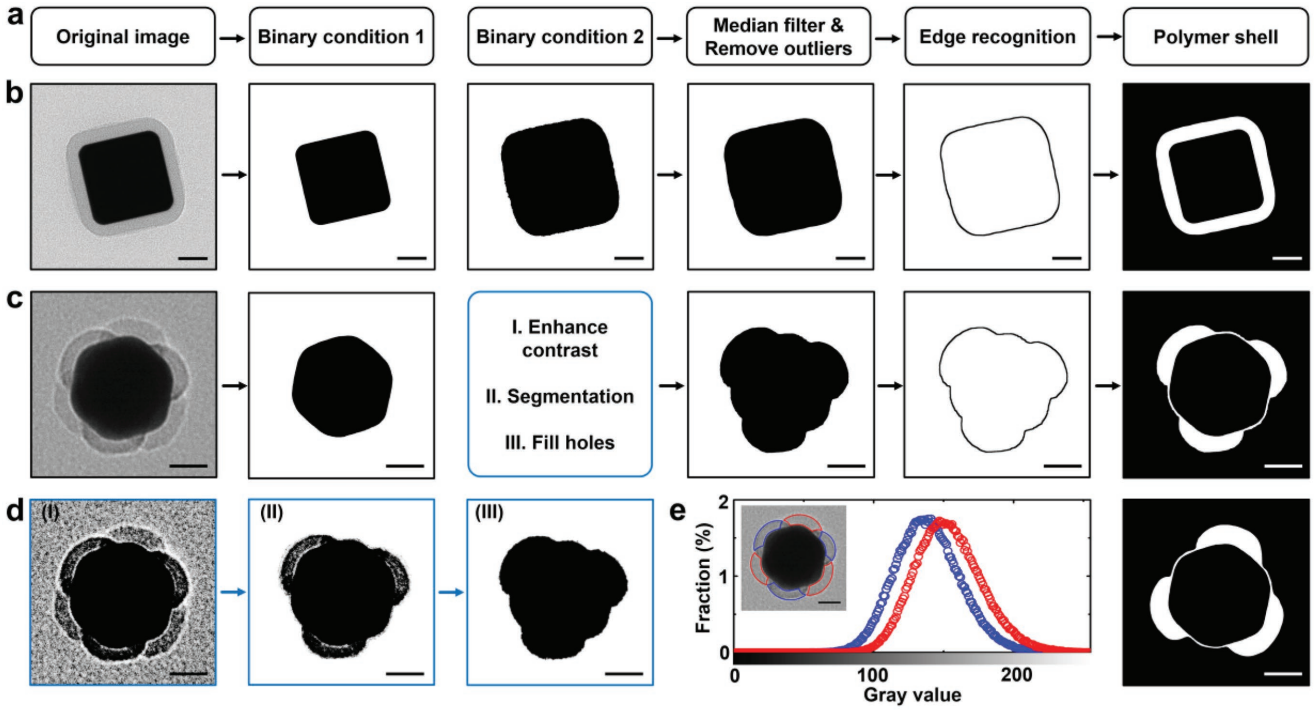

Figure 2. Image processing work flow for the contour curvature analysis of TEM images shown in Figure 1. a) Our generic image analysis protocol. b) Image processing of an as-prepared PS-coated cube. c,d) Image processing of a PS-coated octahedron after polymer shell segregation. The additional steps in d are applied due to different heights of the segregated polymer patches on the gold octahedron. e) Gray value distribution of the six segregated polymer patches at two different heights. The patches outlined with the same color are recognized to be on the same plane. Scale bars: 20 nm.

before.[19,40,41] The PS-*b*-PAA shelling shows a consistently different type of segregation pattern from the PS ones, and also allows compatibility of the hybrid nanoparticles with aqueous solutions. Such compatibility is important to applications such as seeded growth of functional nanoparticles,[42] diagnosis,[43] drug delivery,[44] and photocatalysis.[45]

As shown in **Figure 3**a–c, we first demonstrate the PS-*b*-PAA coating onto a series of gold core shapes including octahedra (as a comparison to the PS shell in Section 2.1.), concave cubes and bipyramids which are different from previous works in morphology (different anisotropy) as well as synthesis method. Briefly, gold cores were first coated with short thiol ligands, 2-naphthalenethiol, via a ligand exchange.[19,40,41] PS-*b*-PAA solution is then added to the particles so that the phenyl group and the PS block are bound via hydrophobic attraction, resulting in PS-*b*-PAA coating (Figure 3a,b). The octahedral particles become soluble in water after coating due to the negatively-charged PAA block (see the inset photo of water suspension in Figure 3c). The UV–Vis spectra show a slight red-shift in the surface plasmon resonance band of the gold octahedra after the polymer coating (Figure 3c), indicating an increase in the refractive index of the medium surrounding the gold core, and thus decreased surface plasmon resonance energy.[46] The TEM images show that the coating works for gold concave cube and bipyramid cores, all in a similar uniform thickness at room temperature when dispersed in water (Figure 3e,f), consistent with previous work on gold spheres and rods.[47]

We find that the PS-*b*-PAA shells on these differently-shaped cores all undergo segregation upon heating at 90 °C, following the common trend of thinning at the vertices and thickening onto flat facets (Figure 3d–f), different from that for the PS shell segregation. In the TEM images overlaid with contours of core particles and PS-*b*-PAA shells, the local shell thickness, after segregation, consistently reaches zero at core surface sites with high local surface curvature (Figure 3g–i). These observations agree with a recent report on PS-*b*-PAA-shelled gold nanorods,[30] yet still generate a rich library of final patch arrangements due to the diverse core shapes we use here. The generic robustness of the trend supports their proposed reconfiguration mechanism: upon heating, the PS-*b*-PAA shell transits to a viscous layer and contracts to reveal high local curvature vertices where dewetting occurs.[30]

Interestingly, the reconfigurability is maintained when we render a further coating of gold seeds onto the PS-*b*-PAA shell periphery, which can serve as growth sites to attach other nanostructures upon. Specifically, we applied to the anisotropically shaped hybrid nanoparticles the literature method of gold seeding used previously on spherical cores upon modification.[48] The PS-*b*-PAA-coated nanoparticles were first incubated with positively charged poly(allylamine hydrochloride), which attract and fasten negatively charged gold seeds (Figure 3j) via electrostatic attraction (Figure 3k). The polymer shell thickness does not alter after the loading of gold seeds. The noncovalent attraction is not expected to alter polymer conformation, and indeed, upon heating, we retrieved the same segregation behaviors in the gold-seeded particles as those in particles that are not coated with gold (Figure 3k,l) which has not been realized before. We foresee

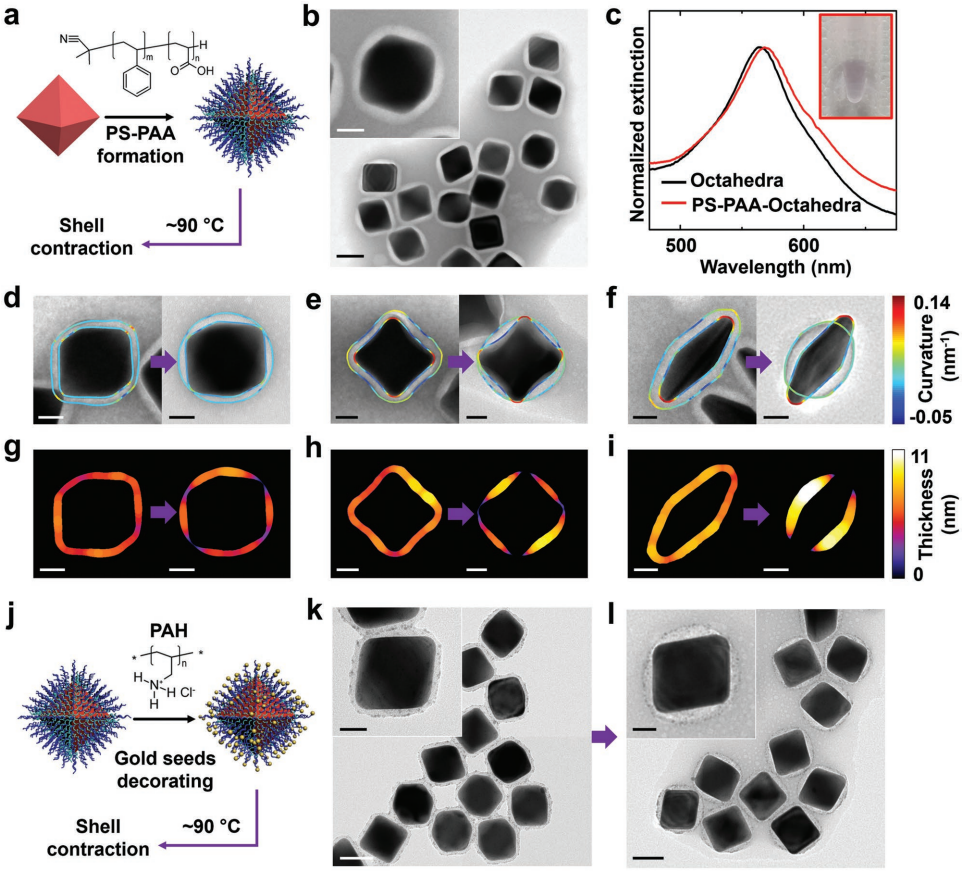

Figure 3. PS-*b*-PAA polymer shell formation, heat-induced reconfiguration and functionalization with gold seeds. a) Schematic of PS-*b*-PAA coating on a gold octahedron and reconfiguration of the polymer shells upon heating (blue: PS-*b*-PAA and dark emerald: 2-naphthalenethiol on the octahedral surface). b) TEM images of PS-*b*-PAA-coated gold octahedra with negative staining (see more details in Section S4, Supporting Information). c) UV–Vis spectra of gold octahedra before (black) and after (red) PS-*b*-PAA coating. The inset picture shows well-dispersed PS-*b*-PAA-coated octahedra in water. d–f) TEM images of a PS-*b*-PAA-coated octahedron, concave cube, and bipyramid particle upon heating, with negative staining. The TEM image after the purple arrow presents the particle after the heating in each panel. The corresponding surface contours are overlaid on the polymer shell and cores. g–i) The local thickness map of the singled-out polymer shell segregation region corresponding to d–f). j) Decoration of PS-*b*-PAA-coated octahedra with gold seeds, which also undergo polymer shell segregation after heating. k,l) TEM images of the PS-*b*-PAA-coated octahedra before and after segregation, both already coated with 2 nm gold seeds. Scale bars: 50 nm for the large-scale images in b, k, and l, and 20 nm for d–f and the inset images in b, k, and l.

more study with different shapes, sizes and further growth of decorating gold seeds, control of the polymer shell thickness and conjugation of other functional groups on the PS-*b*-PAA can help develop hybrid nanomaterials with multiplexed functions.

3. Conclusions

We performed polymer shell coating on a series of anisotropically shaped gold nanoparticles and demonstrate their stimuli-responsive reconfiguration in a highly quantitative manner via analysis of curvature contour and shell thickness. In the PS-coated octahedron and cube, the once uniform polymer shell segregates locally at the vertices and edges, based on the TEM images and tracked surface curvature and thickness distribution. The PS-*b*-PAA-coated nanoparticles (octahedra, concave cubes, and bipyramids), however, display segregation patterns under heating as opposed to the high curvature-oriented segregation in the PS-coated nanoparticles. In addition, the water-processible PS-*b*-PAA-coated nanoparticles can be decorated with gold seeds, which can enrich diversity in such materials properties and functions. Extensions of this work can involve utilization of the novel patch pattern generated here on shape-anisotropic cores for reconfigurable self-assemblies, where the assembly symmetry of the building blocks can be dynamically modulated either by solvent polarity or temperature.

Supporting Information

Supporting Information is available from the Wiley Online Library or from the author.

Acknowledgements

X.S. and A.K. contributed equally to this work. This work was supported by the National Science Foundation under Grant No. 1752517.

Conflict of Interest

The authors declare no conflict of interest.

Keywords

anisotropic nanoparticles, patchy colloids, polymer shell functionalization, reconfigurable nanoparticles, surface segregation, TEM image analysis

Received: February 1, 2018
Revised: March 16, 2018
Published online:

[1] M. A. C. Stuart, W. T. S. Huck, J. Genzer, M. Müller, C. Ober, M. Stamm, G. B. Sukhorukov, I. Szleifer, V. V. Tsukruk, M. Urban, F. Winnik, S. Zauscher, I. Luzinov, S. Minko, *Nat. Mater.* **2010**, *9*, 101.
[2] M. Tagliazucchi, M. G. Blaber, G. C. Schatz, E. A. Weiss, I. Szleifer, *ACS Nano* **2012**, *6*, 8397.
[3] X. Liu, Y. Yang, M. W. Urban, *Macromol. Rapid Commun.* **2017**, *38*, 1700030.
[4] Z. Qian, D. S. Ginger, *J. Am. Chem. Soc.* **2017**, *139*, 5266.
[5] J. Lin, S. Wang, P. Huang, Z. Wang, S. Chen, G. Niu, W. Li, J. He, D. Cui, G. Lu, X. Chen, Z. Nie, *ACS Nano* **2013**, *7*, 5320.
[6] S. Merino, C. Martín, K. Kostarelos, M. Prato, E. Vázquez, *ACS Nano* **2015**, *9*, 4686.
[7] O. S. Muddineti, B. Ghosh, S. Biswas, *Int. J. Pharm.* **2015**, *484*, 252.
[8] H. Jia, J. Cao, Y. Lu, *Curr. Opin. Green Sustainable Chem.* **2017**, *4*, 16.
[9] J. Kao, K. Thorkelsson, P. Bai, B. J. Rancatore, T. Xu, *Chem. Soc. Rev.* **2013**, *42*, 2654.
[10] X. Ye, C. Zhu, P. Ercius, S. N. Raja, B. He, M. R. Jones, M. R. Hauwiller, Y. Liu, T. Xu, A. P. Alivisatos, *Nat. Commun.* **2015**, *6*, 10052.
[11] J. Zhang, P. J. Santos, P. A. Gabrys, S. Lee, C. Liu, R. J. Macfarlane, *J. Am. Chem. Soc.* **2016**, *138*, 16228.
[12] A. H. Groschel, A. Walther, T. I. Lobling, F. H. Schacher, H. Schmalz, A. H. E. Muller, *Nature* **2013**, *503*, 247.
[13] R. M. Choueiri, E. Galati, H. Thérien-Aubin, A. Klinkova, E. M. Larin, A. Querejeta-Fernández, L. Han, H. L. Xin, O. Gang, E. B. Zhulina, M. Rubinstein, E. Kumacheva, *Nature* **2016**, *538*, 79.
[14] E. Galati, M. Tebbe, A. Querejeta-Fernández, H. L. Xin, O. Gang, E. B. Zhulina, E. Kumacheva, *ACS Nano* **2017**, *11*, 4995.
[15] M.-Q. Zhu, L.-Q. Wang, G. J. Exarhos, A. D. Q. Li, *J. Am. Chem. Soc.* **2004**, *126*, 2656.
[16] A. Tokarev, Y. Gu, A. Zakharchenko, O. Trotsenko, I. Luzinov, K. G. Kornev, S. Minko, *Adv. Funct. Mater.* **2014**, *24*, 4738.
[17] C. A. Silvera Batista, R. G. Larson, N. A. Kotov, *Science* **2015**, *350*, 1242477.
[18] M. R. Jones, R. J. Macfarlane, B. Lee, J. Zhang, K. L. Young, A. J. Senesi, C. A. Mirkin, *Nat. Mater.* **2010**, *9*, 913.
[19] H. Wang, X. Song, C. Liu, J. He, W. H. Chong, H. Chen, *ACS Nano* **2014**, *8*, 8063.
[20] N. Kern, D. Frenkel, *J. Chem. Phys.* **2003**, *118*, 9882.
[21] R. L. Marson, T. D. Nguyen, S. C. Glotzer, *MRS Commun.* **2015**, *5*, 397.
[22] V. V. Ginzburg, *Macromolecules* **2017**, *50*, 9445.
[23] M. Tebbe, E. Galati, G. C. Walker, E. Kumacheva, *Small* **2017**, *13*, 1702043.
[24] Z. Nie, D. Fava, E. Kumacheva, S. Zou, G. C. Walker, M. Rubinstein, *Nat. Mater.* **2007**, *6*, 609.
[25] B. Gao, G. Arya, A. R. Tao, *Nat. Nanotechnol.* **2012**, *7*, 433.
[26] C. Tung, A. Cacciuto, *J. Chem. Phys.* **2013**, *139*, 194902.
[27] D. A. Walker, E. K. Leitsch, R. J. Nap, I. Szleifer, B. A. Grzybowski, *Nat. Nanotechnol.* **2013**, *8*, 676.
[28] E. G. Solveyra, M. Tagliazucchi, I. Szleifer, *Faraday Discuss.* **2016**, *191*, 351.
[29] P. J. Flory, *Principles of Polymer Chemistry*, Cornell University Press, Ithaca, NY **1953**.
[30] Z. Wang, G. Xu, G. Wang, Y. Feng, D. Su, B. Chen, H. Zhang, L. Shao, H. Chen, *Nat. Commun.* **2018**, *9*, 563.
[31] M. N. O'Brien, M. R. Jones, K. A. Brown, C. A. Mirkin, *J. Am. Chem. Soc.* **2014**, *136*, 7603.
[32] J. He, Y. Wang, Y. Feng, X. Qi, Z. Zeng, Q. Liu, W. S. Teo, C. L. Gan, H. Zhang, H. Chen, *ACS Nano* **2013**, *7*, 2733.
[33] Y. Feng, Y. Wang, J. He, X. Song, Y. Y. Tay, H. H. Hng, X. Y. Ling, H. Chen, *J. Am. Chem. Soc.* **2015**, *137*, 7624.
[34] J. E. Millstone, W. Wei, M. R. Jones, H. Yoo, C. A. Mirkin, *Nano Lett.* **2008**, *8*, 2526.
[35] S. Torquato, Y. Jiao, *Phys. Rev. E* **2009**, *80*, 041104.
[36] E. B. Zhulina, T. M. Birshtein, V. A. Priamitsyn, L. I. Klushin, *Macromolecules* **1995**, *28*, 8612.
[37] J. Kim, Z. Ou, M. R. Jones, X. Song, Q. Chen, *Nat. Commun.* **2017**, *8*, 761.
[38] Q. Chen, S. C. Bae, S. Granick, *J. Am. Chem. Soc.* **2012**, *134*, 11080.
[39] X. Ye, M. R. Jones, L. B. Frechette, Q. Chen, A. S. Powers, P. Ercius, G. Dunn, G. M. Rotskoff, S. C. Nguyen, V. P. Adiga, A. Zettl, E. Rabani, P. L. Geissler, A. P. Alivisatos, *Science* **2016**, *354*, 874.
[40] L. Zhu, H. Wang, X. Shen, L. Chen, Y. Wang, H. Chen, *Small* **2012**, *8*, 1857.
[41] H. Y. Chen, S. Abraham, J. Mendenhall, S. C. Delamarre, K. Smith, I. Kim, C. A. Batt, *ChemPhysChem* **2008**, *9*, 388.
[42] A. Walther, A. H. E. Müller, *Chem. Rev.* **2013**, *113*, 5194.
[43] J. Song, B. Duan, C. Wang, J. Zhou, L. Pu, Z. Fang, P. Wang, T. T. Lim, H. Duan, *J. Am. Chem. Soc.* **2014**, *136*, 6838.
[44] H. Wang, J. Xu, J. Wang, T. Chen, Y. Wang, Y. W. Tan, H. Su, K. L. Chan, H. Chen, *Angew. Chem., Int. Ed.* **2010**, *49*, 8426.
[45] Z. Huang, Y. Liu, Q. Zhang, X. Chang, A. Li, L. Deng, C. Yi, Y. Yang, N. M. Khashab, J. Gong, Z. Nie, *Nat. Commun.* **2016**, *7*, 12147.
[46] M. Grzelczak, A. Sanchez-Iglesias, L. M. Liz-Marzan, *CrystEngComm* **2014**, *16*, 9425.
[47] H. Wang, L. Chen, Y. Feng, H. Chen, *Acc. Chem. Res.* **2013**, *46*, 1636.
[48] X. Song, C. Liu, S. Liu, W. Xu, *Nano Res. Appl.* **2017**, *3*, 6.